ARTICLE

Nanoscale Zerovalent Iron Supported on Uniform Carbon Microspheres for the In situ Remediation of Chlorinated Hydrocarbons

Bhanukiran Sunkara,[†] Jingjing Zhan,[†] Jibao He,[‡] Gary L. McPherson,[§] Gerhard Piringer,[||] and Vijay T. John*[,†]

Department of Chemical and Biomolecular Engineering, Coordinated Instrumentation Facility, Department of Chemistry, and Department of Earth and Environmental Sciences, Tulane University, New Orleans, Louisiana 70118, United States

ABSTRACT Nanoscale zerovalent iron particles (NZVI) are a preferred option for reductive dehalogenation of dense nonaqueous phase chlorinated hydrocarbons such as trichloroethylene (TCE) because of their environmentally benign nature, high efficiency, and low cost. This study describes an approach to engineered particles containing NZVI that are effective targeted delivery agents for the remediation of these compounds. The particles contain highly uniform carbon microspheres embedded with NZVI (Fe^0/C composite particles). The highly adsorptive carbon keeps the TCE in the proximity of the reactive sites and serves as a sorptive sink for TCE removal. The Fe^0/C composite particles are in the optimal size range for transport through soil and the polyelectrolyte (Carboxymethyl cellulose, CMC) is used to stabilize the composite microspheres in aqueous solution. The multiple functionalities associated with these particles can be designed at low cost and the materials are environmentally benign.

KEYWORDS: carbon microspheres • NZVI • DNAPL • adsorption • carbothermal • trichloroethylene (TCE)

INTRODUCTION

Dense nonaqueous phase liquids (DNAPLs), such as trichloroethylene (TCE) and tetrachloroethene (PCE), are widespread soil and groundwater contaminants that cause long-term environmental pollution. The cleanup of DNAPL contaminated sites is of utmost importance and can be a challenging task due to subsurface heterogeneity and complex site architecture (1, 2). Soil vapor extraction, bioremediation, pump and treat methods, and the in situ placement of reactive metal barriers are some of the various methods developed for the remediation of DNAPLs (3−8). Compared to these approaches, the in situ injection of nanoscale zerovalent iron (NZVI) to reduce DNAPLs is a potentially simple, cost-effective, and environmentally benign technology that become a preferred method in the remediation of these compounds (9, 10).

For successful in situ source remediation of TCE, it is important for the injected remediation agents to effectively migrate through the porous media (11, 12). However, unsupported NZVI particles are chemically unstable and tend to agglomerate because of their high surface energies and intrinsic magnetic interactions, losing chemical reactivity and mobility through the subsurface. Prior studies have shown that nanoiron mobility can be increased dramatically by stabilizing the particles by adsorption of hydrophilic or amphiphilic organic species such as surfactants, vegetable oils, starches, or polyelectrolytes such as carboxymethyl cellulose (CMC) and poly (acrylic acid) (PAA), or triblock copolymers on the NZVI particle surface (13−19). These adsorbed organics enhance steric or electrostatic repulsions between particles to inhibit NZVI aggregation and increase solution stability. Alternatively, activated carbon granules of 1−3 mm size have been used to prevent NZVI aggregation (20, 21). Carbon-based composites are also advantageous because of their high adsorptive capacity. Activated carbons adsorb chlorinated compounds, and these materials have been used in the development of adsorptive-reactive barriers (22).

For effective design of multifunctional colloid particulate systems for in situ TCE remediation, we need to meet several factors. The prepared particulate systems must be able to move through the porous media with optimal mobility, reach TCE contaminated sites, partition to the TCE phase, and break down the contaminant. It would be advantageous if these particles reduce the bulk TCE concentration through sequestration by adsorption followed by reaction during mobility through the subsurface. Additional factors include the following: (1) small amounts of a catalyst, typically palladium are used to dramatically enhance reactivity through dissociative adsorption of H_2 on the catalyst surface (11, 23−25); and (2) the mobility of colloids in the subsurface is determined by competitive mechanisms of Brownian motion, interception by soil and sediment grains and sedimentation effects. The Tufenkji−Elimelch model, which consid-

* Corresponding author. E-mail: vj@tulane.edu. Phone: (504) 865-5883. Fax: (504) 865-6744.

Received for review June 17, 2010 and accepted September 13, 2010

[†] Department of Chemical and Biomolecular Engineering, Tulane University.
[‡] Coordinated Instrumentation Facility, Tulane University.
[§] Department of Chemistry, Tulane University.
[||] Department of Earth and Environmental Sciences, Tulane University.

DOI: 10.1021/am1005282

Published on Web 09/29/2010

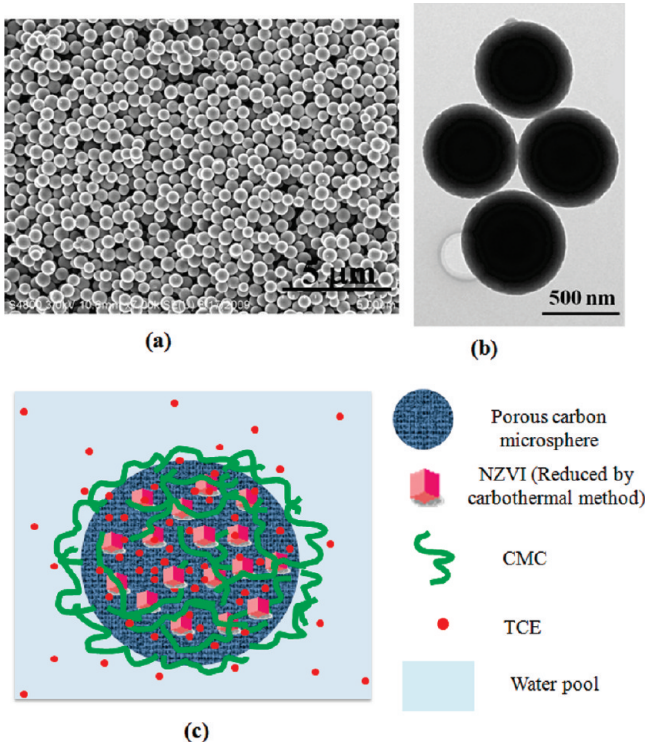

FIGURE 1. (a) SEM and (b) TEM of 500 nm carbon particles obtained from hydrothermal dehydration and pyrolysis of sucrose. (c) Schematic of the multifunctional particulate system showing a NZVI embedded carbon particle with a corona of CMC. The red dots signify TCE in solution and adsorbed on the carbon.

ers the effect of hydrodynamic forces and van der Waals interactions between colloidal particles and sediment grains is a significant improvement over earlier models and predicts that particles in the size range 0.1−1.0 μm have optimal transport properties at typical groundwater flow conditions (19, 26, 27).

In this study, we combine two existing processes for a new approach to the preparation of composite NZVI particles for effective in situ remediation of TCE. The first process is based on the production of highly uniform carbon microspheres through the hydrothermal dehydration of simple sugars followed by carbonization (28−30). These carbon microspheres represent the support for NZVI and their relative monodispersity is shown in images a and b in Figure 1. The second process is that of carbothermal reduction, where iron oxides and hydroxides on the surface of these carbons are reduced to zerovalent iron at temperatures of 800−1000 °C with the accompanying evolution of carbon monoxide and carbon dioxide (31). Carbothermal processes occur during high carbon steel-making processes and have been well-studied (31). In environmental remediation, Hoch and co-workers first applied the principle successfully by reacting soluble iron salts with carbon black to form reactive iron nanoparticles for the remediation of hexavalent chromium (32).

This paper therefore describes a way to combine sugar hydrothermal dehydration and iron oxide/hydroxide carbothermal reduction to synthesize highly uniform colloidal carbon microspheres embedded with NZVI (hereafter called Fe^0/C composite particles), which then are stabilized with a polyelctrolyte (carboxymethyl cellulose) to maintain suspension stability. There are several potentially useful properties of this new composite: (a) supporting the NZVI on carbon is expected to inhibit aggregation of NZVI; (b) in analogy with the adsorptive properties of activated carbon, the carbon microspheres are expected to strongly adsorb TCE, thereby potentially reducing solution TCE content; and (c) the size and monodispersity of the Fe^0/C composite particles may facilitate optimal transport in groundwater. The materials involved are easily available, expected to be environmentally benign, and relatively inexpensive. The hydrothermal dehydration synthesis of the carbon microspheres in solution, and the simple, inexpensive carbothermal reduction for the preparation of Fe^0/C composites would indicate scalability to manufacturing volumes. In addition, the fact that the microspheres are in the optimal size range for transport as predicted by the T−E model (26) and that they can be made with high monodispersity and with inexpensive precursors provides the motivation to test their use in the in situ remediation of TCE.

This work is a direct extension of our recent paper where we have combined carbon microspheres with NZVI that is anchored to the stabilizing polymer (CMC) (33). The current work attempts to illustrate that NZVI can be directly supported on carbon microspheres and that reduction of precursor iron salts to zerovalent iron does not need to take place through addition of a reductant such as sodium borohydridge. Instead, reduction can occur through the carbothermal step to generate NZVI and generating porous carbons. In all experiments, we also add extremely small amounts of Pd (0.1 wt %) to catalyze the dissociative chemisorptions of H_2 (11, 23−25). The system therefore is based on NZVI nanoparticles on carbon microspheres, which are colloidally stabilized by the addition of a polyelectrolyte such as carboxymethyl cellulose (CMC), as shown in Figure 1c. The characteristics of such particles as applied to TCE remediation are the focus of this paper.

EXPERIMENTAL SECTION

Chemicals. All chemicals for synthesis were purchased from Sigma-Aldrich and used as received: Sucrose ($C_{12}H_{22}O_{11}$, ACS reagent), Iron(III) chloride hexahydrate ($FeCl_3 \cdot 6H_2O$, 97%, ACS reagent), sodium carboxymethyl cellulose (NaCMC or CMC, mean MW = 90 000, low viscosity), potassium hexachloropalladate (IV) (K_2PdCl_6, 99%) and trichloroethylene (TCE, 99%). Deionized (DI) water generated with a Barnstead E-pure purifier (Barnstead Co., Iowa) to a resistance of approximately 18 MΩ was used in all experiments.

Preparation of Fe^0/C Composite Particles. Uniform carbon microspheres were prepared from sucrose by hydrothermal treatment which involves two steps, the dehydration of sucrose followed by pyrolysis (carbonization) at high temperatures. The process is similar to that reported in the literature (28, 30) but with minor modifications, and is briefly described. In a typical preparation, a 0.15 M aqueous sucrose solution was dehydrated at 190 °C for 5 h in a sealed stainless steel autoclave filled to 90% capacity. The resulting solid suspension was centrifuged and washed three times with ethanol and air-dried. The material was then pyrolyzed in a tube furnace for 10 h at 1000 °C under flowing argon gas. The resulting carbon microspheres were stored in an airtight vial. The preparation is illustrated on shown through by a flow sheet in Figure 2a.

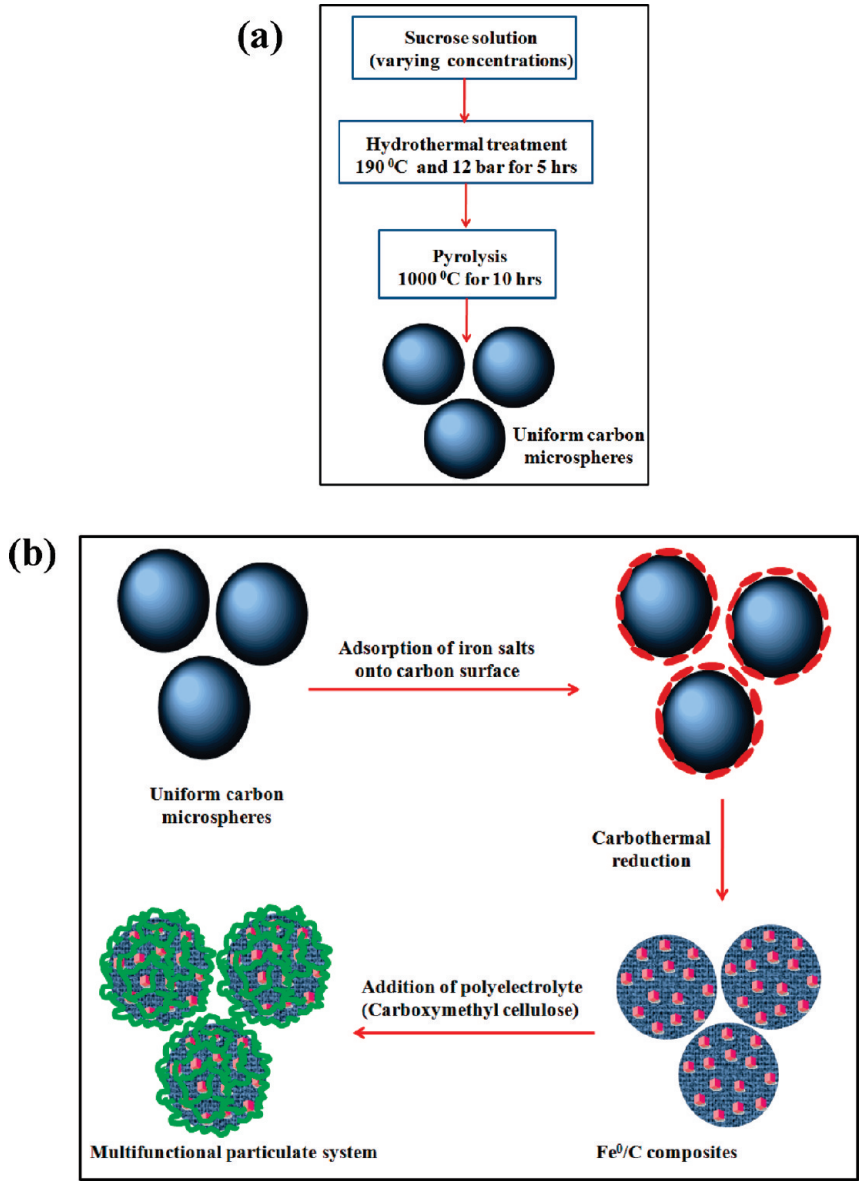

FIGURE 2. (a) Flow sheet for the preparation of uniform monodisperse carbon microspheres. (b) Schematic for the synthesis of multifunctional particulate system.

Carbothermal reduction was employed to synthesize the Fe^0/C composite particles. In a typical synthesis, 0.5 g of the carbon microspheres were first dispersed in 50 mL of water and to this 2.42 g $FeCl_3 \cdot 6H_2O$ salt dissolved in 50 mL water was added and stirred overnight. The solution was then heated at 80 °C to remove the water and then air-dried. The dried particles were pyrolyzed under flowing argon at 800 °C for 3 h to obtain the final Fe^0/C composite particles. To stabilize these composite particles in solution and to enhance their mobility through sediments, 1 % (w/w) CMC was added to 5 g/L Fe^0/C composites in water. The process is shown schematically in Figure 2b. Figure 1c illustrates the concepts behind this study, which shows a schematic of a Fe^0/C composite surrounded by a corona of CMC.

Particle Characterization. Field-emission scanning electron microscopy (SEM, Hitachi S-4800, operated at 20 kV), transmission electron microscopy (TEM; JEOL 2010, operated at 120 kV voltage), and X-ray diffraction (XRD, Rigaku, using Cu Kα radiation) were used to characterize particle size, morphology and crystal structure. Nitrogen Brunauer–Emmet–Teller (BET) adsorption isotherms were obtained using a Micromeritics ASAP 2010 surface area analyzer. Optical microscopy (Olympus IX71, Japan) was used to analyze the behavior of the particles in porous media.

Reaction and Stability Analysis. To test the reactivity of the particles with TCE, we dispersed 0.25 g of Fe^0/C composite particles in 10 mL of water. To this was added 125 μL of 0.0047 M K_2PdCl_6 to load the catalyst Pd onto Fe^0/C composite particles. The catalyst loading is similar to the procedure described in the literature (14, 33–36). The particle suspension was placed in a 40 mL reaction vial capped with a Mininert valve. To this vial was added 10 mL of 40 ppm TCE stock solution to reach an overall concentration of 20 ppm TCE. Accordingly, the final composition of Fe^0/C composite particles used in this study is 3.125 g/L Fe^0, 9.375 g/L carbon, and 0.1 % Pd (w/w of Fe^0). TCE and reaction products were monitored through headspace analysis using a HP 6890 gas chromatograph equipped with a J&W Scientific capillary column (30 m × 0.32 mm) and a flame ionization detector (FID). Samples were injected splitless at 220 °C. The oven temperature was held at 75 °C for 2 min, ramped to 150 °C at a rate of 25 °C/min, and finally held at 150 °C for 10 min to ensure adequate peak separation between TCE and chlorinated and nonchlorinated reaction products.

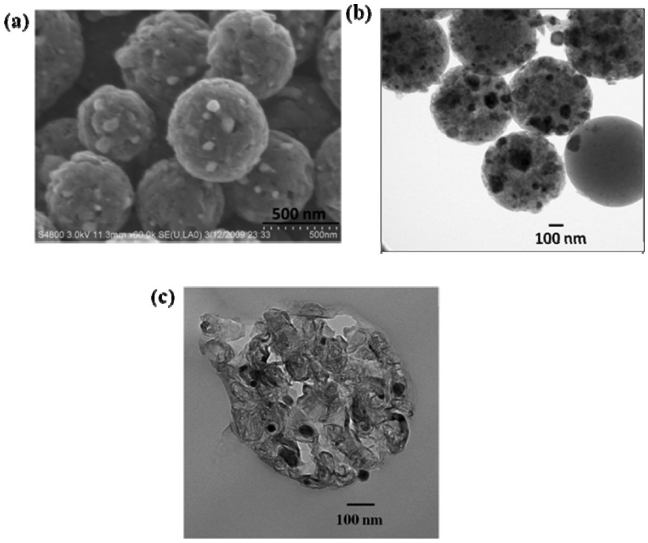

FIGURE 3. (a) SEM and (b) TEM of Fe^0/C composite particles (carbons embedded with NZVI). (c) Cut section TEM of Fe^0/C composite particles (carbons embedded with NZVI).

To determine the minimum amount of CMC required stabilizing the carbon particles in solution for extended time periods, we added varying concentrations of CMC polyelectrolyte systematically to aqueous suspensions of carbon particles. The well-mixed suspensions were added to sample vials and allowed to settle while turbidity measurements were taken over time. The carbon particles were separately dispersed in water by probe sonication for 30 min. Electrolyte (1 mM NaCl) was added to the suspensions to mimic realistic groundwater conditions (37, 38). CMC solution was first added to the dispersed carbon particle solution and mixed for 10 min before the addition of the electrolyte. The concentration of CMC varied from 50 mg/L (0.005%) to 5000 mg/L (0.5%). The final composition of the colloidal suspension was 50 mg/L carbon, 1 mM NaCl and varying concentrations of CMC. The turbidity, measured in nephelometric turbidity units (NTU), was monitered using a benchtop turbidity meter (model DRT-100B, HF Scientific, Inc., Fort Myers, FL). For accuracy, each turbidity measurement was repeated several times and averaged. All turbidity measurements showed good reproducibility. The viscosities of the CMC solutions at various concentrations were measured using a laboratory rheometer (model AR 2000 Rheometer, TA Instruments, USA). The viscosities of the CMC solutions at various concentrations with carbon (50 mg/L) and electrolyte were also measured to note any changes in viscosity with the presence of the additives. Zeta potentials were measured using a Malvern Nanosizer (Malvern Instruments, USA).

RESULTS AND DISCUSSION

Particle Characterization. Scanning and transmission microscopy were used to analyze the morphology and microstructure of the composite particulate system. As shown in images a and b in Figure 1, carbon particles prepared through the hydrothermal method are spherical, uniform, and monodisperse with particle size around 500 nm, consistent with the literature (28). Images a and b in Figure 3 show the carbon microspheres embedded with NZVI particles (Fe^0/C composite particles) obtained after carbothermal reduction process, and the image in Figure 3c is the cut section TEM of an Fe^0/C composite particle showing the presence of NZVI within the porous microspheres. The presence of nanoiron with higher electron

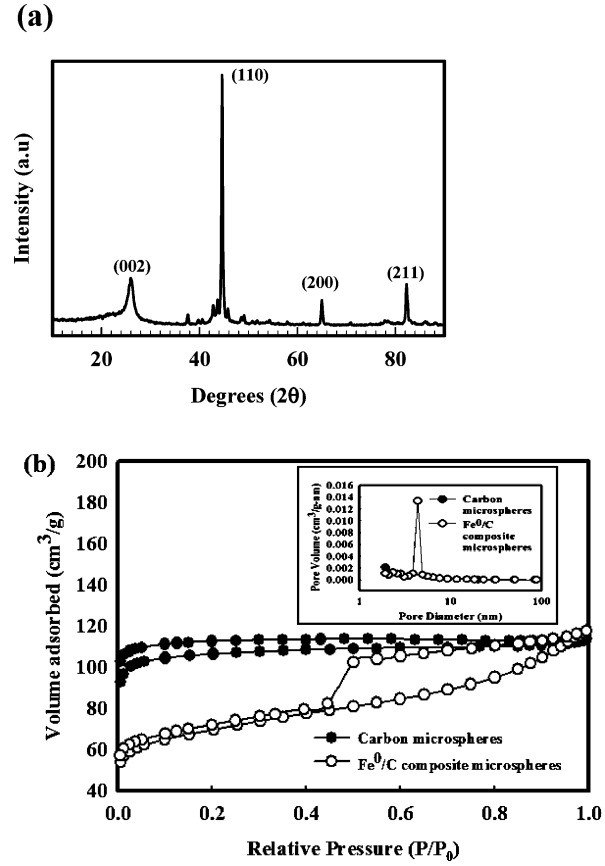

FIGURE 4. (a) XRD pattern of Fe^0/C composite microsphere particles. (b) Nitrogen adsorption−desorption isotherms for the carbon microspheres and Fe^0/C composite microspheres. Inset shows the BJH pore size distribution derived from the desorption branch of the isotherm of carbon microspheres and Fe^0/C composite microspheres.

contrast inside the carbons indicates the distribution of nanoiron throughout the carbon without aggregation. The presence of zerovalent iron is confirmed by the XRD pattern in Figure 4a. In the XRD pattern of Fe^0/C composite particles, the 26° 2θ peak corresponds to 002 graphitic carbon spheres and peaks at 45, 65, and 82° 2θ correspond to zerovalent iron.

Figure 4b shows the N_2 adsorption isotherms obtained for these microspherical particles. Surface areas for the native carbon microspheres and Fe^0/C composite microspheres at 77 K were calculated using Brunauer−Emmet−Teller (BET) method. The BET surface areas were found to be 320 and 221 m^2/g, respectively, and the corresponding Barret−Joyner−Halenda (BJH) desorption pore volumes were determined to be 0.0109 and 0.1282 cm^3/g. The adsorption isotherms are Type I for the carbon microspheres and Type IV for Fe^0/C composite microspheres, using the Brunauer, Demming, Demming, and Teller (BDDT) classification (39). The isotherms indicate a highly microporous structure for carbon microspheres, and a transition to mesopore structure with capillary condensation for the Fe^0/C composite microspheres (40). The transition to mesopore structure for Fe^0/C composite is evident from the BJH pore size distribution, shown in the inset of Figure 4b.

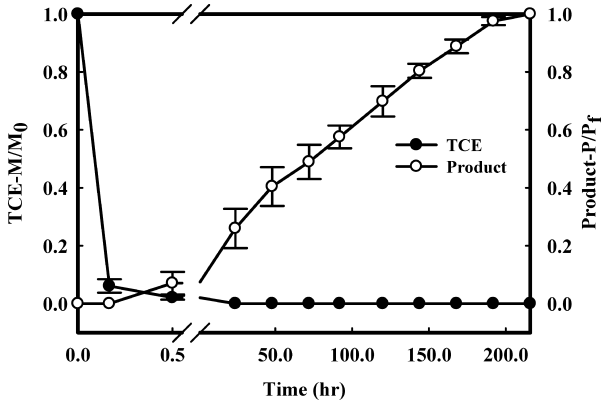

FIGURE 5. TCE removal from solution and gas product evolution rates for Fe^0/C composites (0.25 g particles, and 0.1% Pd (w/w Fe^0). M/M_0 is the fraction of the original TCE remaining and P/P_f is the ratio of the gas product peak to the gas product peak at the end of 9 days. The pseudo first order rate constant is 0.0145 h^{-1}, and the mass normalized rate constant is 4.64 × 10^{-3} L g^{1-} h^{-1}.

The evolution of pore structure is also clearly visualized in TEM images b and c in Figure 3.

Reactivity Characteristics. The reaction kinetics of TCE in the presence of Fe^0/C particles with added palladium is shown in Figure 5. An immediate sharp reduction of the TCE peak is followed by a much slower decline in TCE concentrations. This sharp reduction is not due to reaction but to TCE adsorption on the carbon, as the product generation follows a much slower rate. The subsequent slow evolution of gas phase TCE dechlorination products indicates that dechlorination of TCE is responsible for the second, slower phase in the combined adsorption + reaction sequence. Assuming that dechlorination of TCE is rate controlling for the second step, it is possible to calculate a pseudo-first-order rate constant for TCE dechlorination from the evolution rate of gas phase products. The observed pseudo-first order rate constant was 0.0145 h^{-1} and the mass normalized rate constant, k_m, was 4.64 × 10^{-3} L g^{-1} h^{-1}.

Although the pseudo-first-order rate constant is relatively low, we note that for in situ injection of NZVI-based materials, the reaction rate alone is insufficient to make these materials good remediation candidates (10, 41, 42). In in situ injection, as long as reaction occurs over reasonable time scales, reactive systems can be used as long as they are able to come into contact with TCE saturated groundwater in an effective manner through effective transport in groundwater saturated sediments, and through contaminant sequestration. We are able to enhance the reactivity by 2 orders of magnitude through alternate routes of metal reduction but we will defer this discussion to the section on rate enhancements.

Adsorption Characteristics. The adsorption of TCE on the carbons is a significant advantage of the proposed technology since this property will allow sequestration of the TCE on the reactive materials. We have calculated the partition coefficient for TCE adsorption on the Fe^0/C composite particles using the comprehensive definition of Phenrat and co-workers (41)

$$\frac{C_{TCE}^{ads}}{C_{TCE}^{water}} = K_P = \left\{ \frac{\left[(C_{TCE}^{air})_{ref} V_{hs} - (C_{TCE}^{air})_{ads} V_{hs}\right] + \left[\left(\frac{C_{TCE}^{air}}{K_H^{TCE\bullet}} V_{water}\right)_{ref} - \left(\frac{C_{TCE}^{air}}{K_H^{TCE\bullet}} V_{water}\right)_{ads}\right]}{\left(\frac{M_{ads}}{\rho_{ads}}\right)\left(\frac{C_{TCE}^{air}}{K_H^{TCE\bullet}}\right)_{ads}} \right\}$$

Where C_{TCE}^{ads} is the concentration of TCE on the adsorbent (mol/L), C_{TCE}^{water} is the concentration of TCE in the water phase (mol/L), C_{TCE}^{air} is the concentration of TCE in the headspace (mol/L), V_{hs} and V_{water} are the volumes of the headspace and water, respectively (L), $M_{ads}$is the mass of the adsorbent (g), ρ_{ads} is the density of the adsorbent (g/L). The subscripts ref and ads refer to the system without and with the adsorbent. $K_H^{TCE\bullet}$ is the Henry's law constant for TCE partitioning in water, with a value of 0.343 at 25 °C (3). The measured partition coefficient for TCE adsorption on CMC is 14.5, in close agreement with that measured by Phenrat and co-workers (41). On the other hand, K_p for the adsorption of TCE on Fe^0/C composite particles is 4819, constituting an almost 300 fold increase in adsorption capacity.

Colloidal Stability and Partitioning. The colloidal stability of nano- and microscale particles is a key factor in assessing their transport in groundwater (10). Results of stabilization experiments are illustrated in Figure 6a, showing turbidity as a function of time; NTU_0 indicates the initial

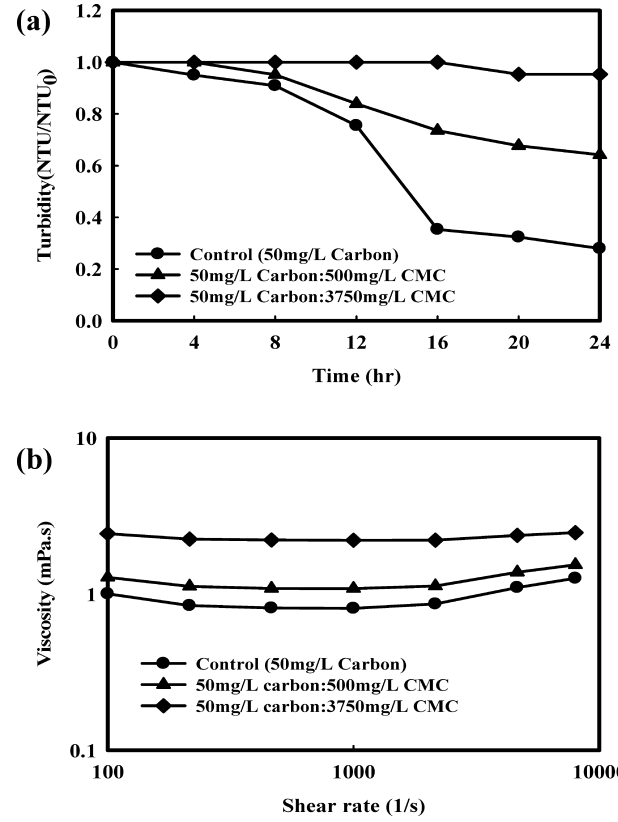

FIGURE 6. (a) Stability of carbon microspheres (500 nm) in various concentrations of carboxymethyl cellulose. (b) Viscosity versus shear rate for various concentrations of carboxymethyl cellulose. (Electrolyte (NaCl) concentration in all experiments is 1 mM).

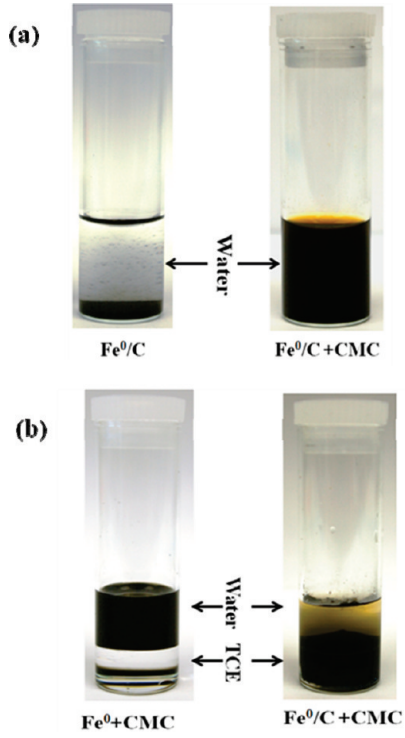

FIGURE 7. (a) Stability of Fe^0/C + CMC in water (b) Partitioning characteristics of Fe^0 + CMC and Fe^0/C + CMC when contacted with a two-phase water−TCE system.

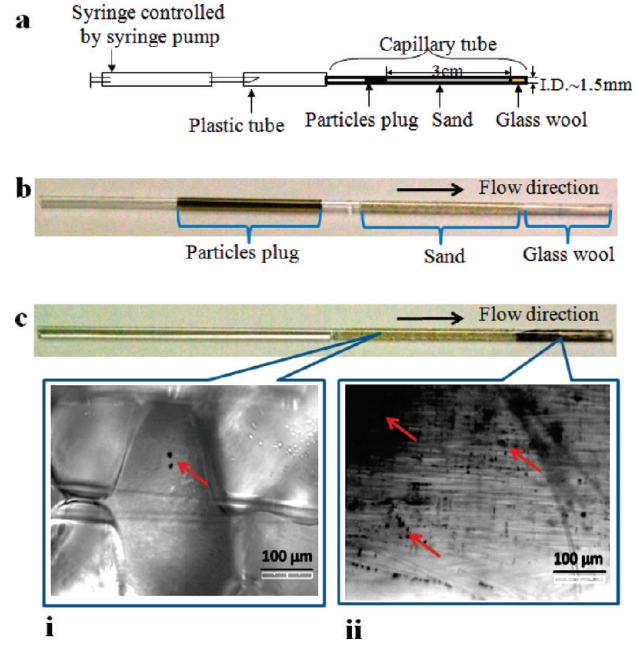

FIGURE 8. Characterization of transport through packed capillaries. (a) Experimental setup. Flow rate, 0.1 mL/min; sand length, 3 cm; and injected suspension volume, 0.03 mL. Photograph of capillary (b) before and (c) after water flushing. Panels i and ii show optical micrographs of sediments and particles at different locations after water flushing (all scale bars are 100 um). Arrows show the accumulated particles in the packed capillary at different locations.

turbidity at time zero. Figure 6a clearly shows that CMC decreases the settling rate of carbon particles, and above a CMC concentration of 2500 mg/L, the carbon particles are stable for more than 24 h. Figure 6b indicates the viscosity versus shear rate for various concentrations of CMC, illustrating no significant increase in viscosity with the CMC concentrations used to stabilize the carbon microspheres and implying no significant difficulty in the injection of these particles into TCE contaminated groundwater.

Figure 7 illustrates simple visual studies of suspension and partitioning characteristics of the carbon-based systems. The samples were probe sonicated to enhance mixing and allowed to equilibrate. Figure 7a illustrates the suspension stability of Fe^0/C samples in water and it is clear that CMC stabilizes the carbon particles. All suspensions were stable in water for more than 4 days, demonstrating the stabilizing effect of CMC as an effective colloid dispersant (15, 32, 36). Figure 7b illustrates the partitioning behavior of carbon when a bulk TCE phase is in contact with a bulk aqueous phase. On the left, the aqueous-phase solution containing Fe^0 + CMC retains suspension stability in the aqueous phase. However, on the right, we see that Fe^0/C + CMC particles partition to the TCE phase and a close inspection indicates that the partitioning is primarily around the TCE side of the water-TCE interface, with a dense layer near the interface. This is clearly a consequence of the tendency of the hydrophobic carbon to partition to the organic phase. The idealized system of a hydrophobic carbon microsphere enveloped by hydrophilic CMC approximates a 500 nm particle with amphiphilic characteristics. This property of partitioning to the interface when in contact with bulk TCE may be of specific advantage in anchoring the particles to pooled TCE at fractures along the sediment-bedrock boundary.

Transport Characteristics. Transport characteristics of Fe^0/C + CMC system were studied by capillary transport experiments. The experiment followed the procedure described by Zhan and co-workers which is a simple and intuitive method to study particle transport through porous media (27). Briefly, glass melting-point tubes with both ends open (1.5−1.8 mm i.d. × 100 mm length, Corning, NY) were used as capillaries. The capillary tubes were packed with wet Ottawa sand over a 3 cm length and were placed horizontally to simulate groundwater flow. A continuous water flow at 0.1 mL/min (Darcy velocity: 5 cm/min) was driven by a syringe pump. The exit point of the capillary was capped with a small glass wool plug. After 30 μL of Fe^0/C + CMC suspension was injected into the inlet of the capillary, water flushing was initiated and an inverted optical microscope was used to observe the pore-scale transport of the particles. Figure 8 illustrates photographs of the capillaries depicting the capillary containing Fe^0/C + CMC colloids before and after the water flush. The images indicate that Fe^0/C composite particles readily transport through the packed capillaries and become captured in the glass wool. The effluent particle concentration was obtained by monitoring the turbidity of elutes with a nephelometric turbidimeter (DRT100B, HF Scientific, Inc., Fort Myers, FL.). In the experiment, particles retained by the glass wool were collected by a simple water washing method and were counted as a part of effluent. The turbidity result indicates that almost all of the Fe^0/C composite particles were eluted from the Ottawa sand capillary under the specified conditions.

In classical colloidal filtration theory (CFT), Brownian diffusion, interception and gravitational sedimentation are the mechanisms that govern the mobility of colloidal particles through porous media such as soil (43). The Tufenkji-Elimelech model is perhaps the most comprehensive model to describe these effects in the presence of interparticle attractive interactions (26). The mobility of particles through porous media is quantified through the collector efficiency η_0, which is simply defined as the ability of the sediment to collect migrating particles, thus limiting transport through the subsurface. According to CFT, the optimal mobility through sediment corresponds to minimal collector efficiency, which typically occurs at a broad particle size range from about 0.2 to 1 μm depending on the particle physical properties and groundwater flow characteristics (19, 26, 27). However, CFT can break down under conditions of deposition in the secondary minimum and surface charge heterogeneities, when consideration of repulsive DLVO interactions are accounted for, as shown by Tufenkji and Elimelech (44, 45). Nevertheless, it is noteworthy that our experimental results do indicate effective transport of the 500 nm composite particles. Additionally, the use of carboxymethylcellulose (CMC) as an anionic polyelectrolyte to stabilize the carbons leads to a high surface charge on the particles. The measured zeta potential is of the order of −45 mV, indicating that the CMC will be able to mask the role of surface heterogeneities and provide better agreement with the modified colloid filtration theory (26).

We have calculated the attachment efficiency (α) (26, 46) from capillary column breakthrough data for 500 nm size Fe^0/C composite particles following the procedure of Zhan and co-workers (33). Briefly, the attachment efficiency (α) is estimated from breakthrough data of capillary transport experiments using the following equations based on CFT (26, 46)

$$\alpha = \frac{-2}{3}\frac{d_c}{(1-f)L\eta_0}\ln(C/C_0)$$

Where d_c is the average diameter of sand grains, C and C_0 are effluent and influent particle concentration, f the porosity of the sand grains, and L the length of the column. η_0, the single-collector efficiency, is calculated using the T−E equation (26)

$$\eta_0 = 2.4A_S^{1/3}N_R^{-0.081}N_{Pe}^{-0.715}N_{vdW}^{0.052} + 0.55A_SN_R^{1.675}N_A^{0.125} + 0.22N_R^{-0.24}N_G^{1.11}N_{vdW}^{0.053}$$

We calculated the attachment efficiency based on the following conditions: porosity, $f = 0.32$; fluid viscosity, $\mu = 1.0 \times 10^{-3}$ N s/m^2; temperature, $T = 298$ K; Hamaker constant (47), $H = 1.09 \times 10^{-19}$ J; density of Fe^0/C composite particles (calculated), $\rho = 2.74$ g/mL $= 2.74 \times 10^3$ kg/m^3; particle size, $d_p = 500$ nm; volumetric flow rate = 0.1 mL/min = 8.3×10^{-4} m/s.

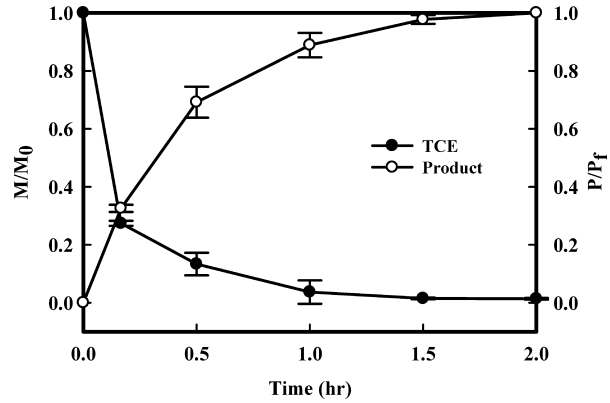

FIGURE 9. TCE removal from solution and gas product evolution rates for Fe^0/C composites prepared by incipient wetness method (20 ppm TCE, Fe^0 concentration 10 g/L, and 0.1% Pd (w/w Fe^0). M/M_0 is the fraction of the original TCE remaining and P/P_f is the ratio of the gas product peak to the gas product peak at the end of 120 min. The first-order rate constant is 2.95 h^{-1} and mass normalized rate constant is 295 $\times$ 10^{-3} L g^{1-} h^{-1}.

With a measured eluting fraction $C/C_0 = 0.97$, the attachment efficiency is 0.0844, indicating effective transport through the packed capillary.

Reaction Rate Enhancements. The reactivity of the carbon supported nanoscale ZVI composites can be enhanced through the addition of sodium borohydride as reducing agent to obtain ZVI nanoparticles, thus avoiding the carbothermal process. First, nanoscale zerovalent iron particles supported on carbon (hereafter called NZVI/C composite particles) microspheres were prepared by the incipient wetness method (48−51), typically used in the preparation of supported catalysts and recently, in reactive barrier design for the dechlorination of polychlorinated biphenyl s (52). In the current study, carbons obtained from the hydrothermal treatment were used and 1:1 weight ratio of carbon to iron was selected for these composite particles. In a typical preparation, 1.936 g of $FeCl_3 \cdot 6H_2O$, dissolved in 5 mL of water, was added to 0.4 g of carbon powder. The volume of the water was kept to a minimum, sufficient enough to wet the solid carbon powder but with no excess liquid present; therefore, it is assumed that all the iron salt particles are dispersed over the solid carbon. The water was then evaporated, leaving a dispersed carbon/iron salt/metal oxide mixture. The dried powder was then reduced with 10 mL of sodium borohydride solution and washed three times with water to obtain NZVI/C composite microspheres. Figure 9 shows the reaction characteristic of NZVI/C particles loaded with 0.1% palladium catalyst (w/w NZVI) prepared by this method. The pseudo first order rate constant is 2.95 h^{-1} and mass normalized rate constant, k_m is 295 $\times$ 10^{-3} L g^{-1} h^{-1}. The reactivity is greater than by a factor of about 60 compared to Fe^0/C composites prepared by the carbothermal process. In all cases, the mass normalized rate constant is calculated based on the weight of iron in the system. Although the use of $NaBH_4$ enhances reaction rate, the cost of the reductant makes is perhaps less economical than the carbothermal method. In continuing work, we seek to understand the variations in reactivity using various reduction methods using detailed X-ray diffraction and X-ray

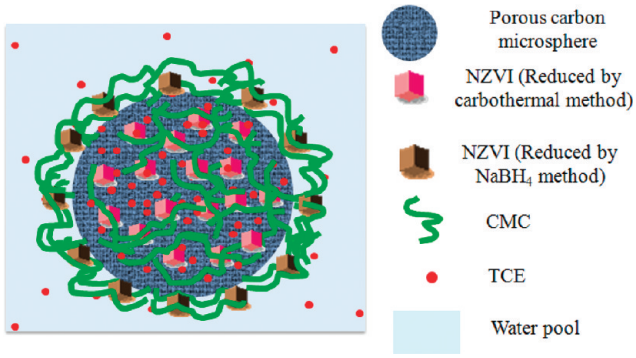

FIGURE 10. Schematic of the multifunctional particulate system showing a NZVI (red cubes) embedded carbon particle surrounded by CMC containing NZVI (brown cubes). The red dots signify TCE in solution and adsorbed on the carbon.

photoelectron spectrosopy (XPS) to understand bulk and surface chacteristics of the different iron species.

Figure 10 summarizes the various configurations of NZVI placement. From our earlier work (33) following the remarkable concepts of Zhao and co-workers (36), we have shown that it is possible to attach NZVI directly to carboxymethyl cellulose (the brown cubes in Figure 10) with high rate constants in the order of 2100×10^{-3} L g^{-1} h^{-1}. The current work describes the placement of NZVI directly on the carbon but with accompanying lower reaction rates. Figure 10 illustrates that it is possible to couple the various configurations to maximize loading. Since NZVI is not a catalyst but becomes gradually oxidized, the combination of slow and fast reacting NZVI may be of advantage in tuning the remediation to contaminant site characteristics.

SUMMARY

In all cases described in this work, the composite materials have multiple functionalities: (a) they are reactive and function effectively in reductive dehalogenation; (b) they are highly adsorptive, thereby bringing the chlorinated compound to the proximity of the reactive sites and also serving as adsorption materials for decontamination; (c) they are in the optimal size range predicted by colloidal filtration theory for optimal transport through sediments; and (d) the composite with a hydrophilic corona and a hydrophobic core may possess amphiphilic properties to stabilize the particles when they reach target zones of bulk DNAPLs. These multiple functionalities can be designed at low cost and the materials are intuitively environmentally innocuous because they contain carbon, iron, and a biodegradable polymer. Although this work is a follow up to our earlier work where NZVI was attached to the polyelectrolyte (33), it considerably expands the scope of the technology through placement of NZVI within the carbon and through the generation of highly adsorptive porous materials.

Acknowledgment. Funding from the Environmental Protection Agency (EPA-GR832374) and the National Science Foundation (Grant 0933734) is gratefully acknowledged. We also acknowledge additional funding from the Advanced Materials Research Institute of the University of New Orleans.

REFERENCES AND NOTES

(1) Al-abed, S. R.; Chen, J. In *Physicochemical Groundwater Remediation*; Smith, J. A., Burns, S. E., Eds.; Kluwer Academic/Plenum: New York, 2001; pp 91−114.
(2) Saleh, N.; Sirk, K.; Liu, Y.; Phenrat, T.; Dufour, B.; Matyjaszewski, K.; Tilton, R. D.; Lowry, G. V. *Environ. Eng. Sci.* **2007**, *24*, 45–57.
(3) Heron, G.; Christensen, T. H.; Enfield, C. G. *Environ. Sci. Technol.* **1998**, *32*, 1433–1437.
(4) Mackay, D. M.; Cherry, J. A. *Environ. Sci. Technol.* **1989**, *23*, 630–636.
(5) Nakano, Y.; Hua, L.; Nishijima, W.; Shoto, E.; Okada, M. *Wat. Res.* **2000**, *34*, 4139–4142.
(6) O'Hannesin, S. F.; Gillham, R. W. *Ground Water* **1998**, *36*, 164–170.
(7) Ritter, K.; Odziemkowski, M. S.; Gillham, R. W. *J. Contam. Hydrol.* **2002**, *55*, 87.
(8) Scherer, M. M.; Richter, S.; Valentine, R. L.; Alvarez, P. J. J. *Crit. Rev. Environ. Sci. Technol.* **2000**, *30*, 363.
(9) Elliott, D. W.; Zhang, W. X. *Environ. Sci. Technol.* **2001**, *35*, 4922–4926.
(10) Phenrat, T.; Saleh, N.; Sirk, K.; Tilton, R.; Lowry, G. *Environ. Sci. Technol.* **2007**, *41*, 284–290.
(11) Nyer, E. K.; Vance, D. B. *Ground Water Monit. Remediat.* **2001**, *2*, 41–46.
(12) Zheng, T.; Zhan, J.; He, J.; Day, C.; Lu, Y.; McPherson, G. L.; Piringer, G.; John, V. T. *Environ. Sci. Technol.* **2008**, *42*, 4494–4499.
(13) Alessi, D.; Li, Z. *Environ. Sci. Technol.* **2001**, *35*, 3713–3717.
(14) He, F.; Zhao, D. *Environ. Sci. Technol.* **2005**, *39*, 3314–3320.
(15) He, F.; Zhao, D. *Environ. Sci. Technol.* **2007**, *41*, 6216–6221.
(16) Kanel, S. R.; Choi, H. *Water Sci. Technol.* **2007**, *55*, 157–162.
(17) Quinn, J.; Geiger, C.; Clausen, C.; Brooks, K.; Coon, C.; O' Hara, S.; Krug, T.; Major, D.; Yoon, W.; Gavaskar, A.; Holdsworth, T. *Environ. Sci. Technol.* **2005**, *39*, 1309–1318.
(18) Saleh, N.; Phenrat, T.; Sirk, K.; Dufour, B.; Ok, J.; Sarbu, T.; Matyiaszewski, K.; Tilton, R. D.; Lowry, G. V. *Nano Lett.* **2005**, *5*, 2489–2494.
(19) Schrick, B.; Hydutsky, B. W.; Blough, J. L.; Mallouk, T. E. *Chem. Mater.* **2004**, *16*, 2187–2193.
(20) Lubick, N. *Environ. Sci. Technol.* **2009**, *43*, 235–235.
(21) Choi, H.; Agarwal, S.; Al-Abed, S. R. *Environ. Sci. Technol.* **2009**, *43*, 488–493.
(22) Al-Abed, S. R.; Jegadeesan, G.; Scheckel, K. G.; Tolaymat, T. *Environ. Sci. Technol.* **2008**, *42*, 1693–1698.
(23) Muftikian, R.; Fernando, Q.; Korte, N. *Water Res.* **1995**, *29*, 2434–2439.
(24) Schreier, C.; Reinhard, M. *Chemosphere* **1995**, *31*, 34753487.
(25) Wang, C.; Zhang, W. *Environ. Sci. Technol.* **1997**, *31*, 2154–2156.
(26) Tufenkji, N.; Elimelech, M. *Environ. Sci. Technol.* **2004**, *38*, 529–536.
(27) Zhan, J.; Zheng, T.; Piringer, G.; Day, C.; McPherson, G. L.; Lu, Y.; Papadopoulos, K.; John, V. T. *Environ. Sci. Technol.* **2008**, *42*, 8871–8876.
(28) Wang, Q.; Li, H.; Chen, L.; Huang, X. *Carbon* **2001**, *39*, 2211–2214.
(29) Wang, Q.; Li, H.; Chen, L. Q.; Huang, X. J. *Solid State Ionics* **2002**, *152*, 43–50.
(30) Yang, R.; Qiu, X.; Zhang, H.; Li, J.; Zhu, W.; Wang, Z.; Huang, X.; Chen, L. *Carbon* **2005**, *43*, 11–16.
(31) L'Vov, B. V. *Thermochim. Acta* **2000**, *360*, 109–120.
(32) Hoch, L. B.; Mack, E. J.; Hydutsky, B. W.; Hershman, J. M.; Skluzacek, I. M.; Mallouk, T. E. *Environ. Sci. Technol.* **2008**, *42*, 2600–2605.
(33) Zhan, J.; Sunkara, B.; Le, L.; John, V. T.; He, J.; McPherson, G. L.; Piringer, G.; Lu, Y. *Environ. Sci. Technol.* **2009**, *43*, 8616–8621.
(34) Grittini, C.; Malcomson, M.; Fernando, Q.; Korte, N. *Environ. Sci. Technol.* **1995**, *29*, 2898–2900.
(35) He, F.; Zhao, D. *Appl. Catal., B* **2008**, *84*, 533–540.
(36) He, F.; Zhao, D.; Liu, J.; Roberts, C. B. *Ind. Eng. Chem. Res.* **2007**, *46*, 29–34.
(37) Atekwana, E. A.; Richardson, D. S. *Hydrol. Process.* **2004**, *18*, 2801–2815.
(38) Busenberg, E.; Plummer, L. N.; Doughten, M. W.; Widman, P. K.; Bartholomay, R. C. *Chemical and Isotopic Composition and Gas Concentrations of Groundwater and Surface Water from Selected Sites at and near the Idaho National Engineering and Environmental*

Laboratory, 1994-1997; U.S. Geological Survey Open-File Report 00-81; U.S. Geological Survey: Reston, VA, 2000.
(39) Brunauer, S.; Deming, L. S.; Deming, W. E.; Teller, E. *J. Am. Chem. Soc.* **2002**, *62*, 1723–1732.
(40) Lowell, S.; Shields, J. E.; Thomas, M. A.; Thommes, M. *Characterization of Porous Solids and Powders: Surface Area, Pore Size and Density*; Kluwer Academic Publishers: Dordrecht, The Netherlands, 2004; pp 11−14.
(41) Phenrat, T.; Liu, Y. Q.; Tilton, R. D.; Lowry, G. V. *Environ. Sci. Technol.* **2009**, *43*, 1507–1514.
(42) Phenrat, T.; Saleh, N.; Sirk, K.; Kim, H. J.; Tilton, R. D.; Lowry, G. V. *J. Nanopart. Res.* **2008**, *10*, 795–814.
(43) Yao, K.-M.; Habibian, M. T.; O'Melia, C. R. *Environ. Sci. Technol.* **1971**, *5*, 1105–1112.
(44) Tufenkji, N.; Elimelech, M. *Langmuir* **2004**, *20*, 10818–10828.
(45) Tufenkji, N.; Elimelech, M. *Langmuir* **2005**, *21*, 841–852.
(46) Saleh, N.; Kim, H.-J.; Phenrat, T.; Matyjaszewski, K.; Tilton, R. D.; Lowry, G. V. *Environ. Sci. Technol.* **2008**, *42*, 3349–3355.
(47) Hartley, P. A.; Parfitt, G. D. *Langmuir* **1985**, *1*, 651–657.
(48) Bowker, M.; Nuhu, A.; Soares, J. *Catal. Today* **2007**, *122*, 245–247.
(49) Itoh, M.; Saito, M.; Takehara, M.; Motoki, K.; Iwamoto, J.; Machida, K.-i. *J. Mol. Catal. A: Chem* **2009**, *304*, 159–165.
(50) Li, Y.; Chen, Y.; Li, L.; Gu, J.; Zhao, W.; Li, L.; Shi, J. *Appl. Catal., A* **2009**, *366*, 57–64.
(51) Pooya, A.; Farnood, R.; Meier, E. *J. Phys. Chem. A* **2010**, *114*, 3962–3968.
(52) Choi, H.; Al-Abed, S. R.; Agarwal, S.; Dionysiou, D. D. *Chem. Mater.* **2008**, *20*, 3649–3655.

AM1005282